

# Pattern formation upon femtosecond laser ablation of transparent dielectrics

Ionut Georgescu\* and Michael Bestehorn

*LS Theoretische Physik II, Brandenburg University of Technology, Erich-Weinert Str. 1, 03046 Cottbus, Germany*

Florenta Costache and Jürgen Reif

*LS Experimentalphysik II, Brandenburg University of Technology, Universitätsplatz 3-4, 03044 Cottbus, Germany*

(Dated: October 16, 2019)

Costache et al. have reported recently a new type of periodic patterns generated at femtosecond laser ablation of transparent dielectrics (Appl. Surf. Sci. **186**, 352(2002)). They show features known from other pattern forming systems far from equilibrium, like point and line defects or grain boundaries, and cannot be explained by the classical theory. The present work is an attempt to investigate these pattern by means of a generalized Kuramoto-Shivashinsky equation derived from the Bradley et al. and Cuerno et al. model for ripple formation at ion beam sputtering of surfaces.

Laser induced periodic surface structures (LIPSS) have been observed for almost 40 years [1] on targets made of intrinsic and extrinsic semiconductors, metals and dielectrics, using cw to subpicosecond laser sources with wave lengths varying from the ultraviolet up to the infrared domain ([2] and references therein, [3, 4, 5]). They have therefore been considered to be a universal phenomenon that can occur on any material that absorbs radiation, regardless of its dielectric constant [1].

The explanation accepted today on a large scale has been delivered by the group of Sipe, Young, Preston, and van Driel [2] in 1983, by taking into account the details of the interaction of an electromagnetic wave with the microscopically rough selvedge of a surface. Thus, the periodic surface structures are the result of the interference between the incoming laser light, the light refracted by the bulk and the light scattered by the rough selvedge (or interface). The aspect of the surface is usually a combination of several basic patterns. For *p*-polarized light, these are the *s*-type patterns (Eq. (1)) perpendicular to the electric field  $\vec{E}$  and the *c*-type patterns parallel to  $\vec{E}$ ; for *s*-polarized light, there are *c*-type patterns perpendicular to  $\vec{E}$  and other patterns with no simple dependence on  $\theta$ , the angle of incidence. Excellent agreement with experimental work that followed [3, 4] has been found.

$$\text{s-type: } \Lambda = \frac{\lambda}{1 \pm \sin \theta}, \quad \text{c-type: } \Lambda = \frac{\lambda}{\cos \theta}. \quad (1)$$

$\lambda$  denotes here the wave length of the laser and  $\Lambda$  the periodicity of the patterns.

Recently, Costache et al. have reported upon a new type of periodic patterns generated at femtosecond laser ablation of transparent dielectrics [6]. These new structures exhibit fundamental differences when compared to the “classical” periodic patterns, such as spacing almost twice as small, independent on the wave length and on the angle of incidence of the laser beam, but correlated with the local incident intensity. Features like point and line defects or grain boundaries can also not be described

by the classical theory. They point rather to a self-organizing mechanism.

The qualitative and quantitative similarities to the patterns observed in ion beam sputtering [17], as well as the wide acceptance of their theoretical description as proposed by Bradley and Harper [7] and Cuerno and Barabási [8], have determined us to use this framework for studying the new structures.

The experiments [6, 9, 10, 11] have been carried out under high vacuum ( $< 10^{-7}$  mbar) on freshly cleaved single crystal slides of BaF<sub>2</sub> and CaF<sub>2</sub>. The laser system generated a pulse of 120 fs with a central wave length of 800 nm and intensities of  $1 - 12 \times 10^{12}$  W/cm<sup>2</sup>. Additionally, the frequency of the laser radiation could be doubled and the angle of incidence of the laser beam on the target could be varied.

The main feature which distinguishes these new structures from the *classical* ones is the spacing. In the classical model the patterns are uniformly distributed across the ablation area, with spacings given by Eq. (1). In this case, however, no dependency of the ripples periodicity on the laser wave length or on the angle of incidence could be observed. Moreover, the periodicity is obviously dependent on the local intensity of the laser beam, as shown in Fig. 1(a). The spacing of the ripples increases here towards the center of the ablation spot, that is, increases with the local intensity. While Eq. (1) allows a minimum spacing of  $\approx 468$  nm for the situation shown in Fig. 1(a), the spacing at the boundary of the ablation spot is approximatively 250 nm.

The model presented by Bradley and Harper [7] and further developed by Cuerno and Barabási [8] is based on Sigmund’s theory of sputtering [12]. Here, an ion striking a solid will first travel a certain distance  $a$ , called average depth of energy deposition, and then lose its energy in a cascade of random atomic collisions. For an ion traveling along the  $z$ -axis, the resulting profile of the average energy deposition in the material ( $z \leq h(x, y)$ ) follows in

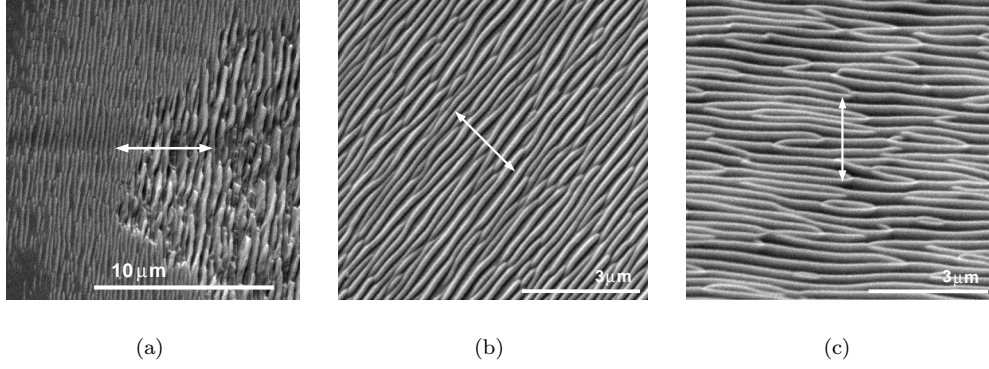


FIG. 1: Orientation of the periodic ripple structure with respect to the laser beam polarization. (a) Ablated spot obtained after 9200 shots at  $0.8 \times 10^{13}$  W/cm<sup>2</sup>; (c) 5000 shots at  $1.2 \times 10^{13}$  W/cm<sup>2</sup>; (a), (b) and (c) 800 nm, 45° incidence.

a good approximation a Gaussian distribution [12]

$$F_D(\vec{r}) = \frac{\epsilon}{(2\pi)^{3/2}\alpha\beta^2} \times \exp \left[ -\frac{[z+a]^2}{2\alpha^2} - \frac{x^2+y^2}{2\beta^2} \right]. \quad (2)$$

$F_D(\vec{r})$  denotes here the energy deposition per unit volume,  $\epsilon$  is the total energy deposited by the ion and  $\alpha$  and  $\beta$  are the widths of the distribution parallel and perpendicular to the plane of incidence, respectively. The erosion velocity at a certain point on the surface is then proportional to the total energy deposited there by the ions within the range  $\mathcal{R}$  of the distribution (2)

$$v(O) \cong \Lambda \int_{\mathcal{R}} \Psi(\vec{r}) F_D(\vec{r}) d\vec{r}, \quad (3)$$

where  $\Psi(\vec{r})$  is the local flux of ions and  $\Lambda$  is a material constant.

Eq. (2) was written in the reference frame of the incoming ion, having the origin at the point of impact  $O$  and the  $z$ -axis pointing away from the surface, along the velocity  $\vec{v}$  of the ion. In Eq. (3) we went over to the local reference frame, with the origin also at  $O$  but with the  $z$ -axis pointing along the surface normal. And finally, there is the reference frame of the laboratory, our destination.

To evaluate the erosion velocity (3), we make the transform  $x \rightarrow a\zeta_x$ ,  $y \rightarrow a\zeta_y$  and expand the integrand in powers of  $a/R_X$  and  $a/R_Y$ .  $R_X$  and  $R_Y$  are the curvature radii at  $O$  and are used to describe the integration region  $\mathcal{R}$

$$h \cong -\frac{1}{2} \left( \frac{x^2}{R_X} + \frac{y^2}{R_Y} \right) \quad (4)$$

with  $1/R_X = -\partial^2 h / \partial x^2$  and  $1/R_Y = -\partial^2 h / \partial y^2$ . After evaluating the resulting Gaussian integrals we make the transition to the laboratory coordinate frame  $(x, y, h)$  [8, 13]

$$\frac{\partial h(x, y, t)}{\partial t} = -v(\phi, R_X, R_Y) \sqrt{1 + (\nabla h)^2} \quad (5)$$

and obtain thus for  $\alpha = \beta$  Cuerno and Barabási's equation of motion [8]

$$\begin{aligned} \frac{\partial h}{\partial t} = & -v_0 + \mu \frac{\partial h}{\partial x} + \nu_x \frac{\partial^2 h}{\partial x^2} + \nu_y \frac{\partial^2 h}{\partial y^2} + \frac{\lambda_x}{2} \left( \frac{\partial h}{\partial x} \right)^2 + \\ & \frac{\lambda_y}{2} \left( \frac{\partial h}{\partial y} \right)^2 - K \nabla^2 (\nabla^2 h) + \eta(x, y, t). \end{aligned} \quad (6)$$

In Eq. (5)  $\phi$  denotes the angle between the incident beam and the surface normal at  $O$ . It can be expressed as a function of the angle of incidence  $\theta$  and the local gradient  $\nabla h$  and can be expanded in powers of the latter.

Eq. (6) has the form of the Kuramoto-Shivashinsky (KS) equation [14].  $v_0$ ,  $\mu$ ,  $\nu_x$ ,  $\nu_y$ ,  $\lambda_x$  and  $\lambda_y$  are functions of the angle of incidence  $\theta$ . The term  $-K \nabla^2 (\nabla^2 h)$  accounts for the surface self-diffusion and  $\eta(x, y, t)$  is a Gaussian white noise, accounting for the stochastic arrival of the ions on the surface. If the surface diffusion is thermally activated, the coefficient  $K$  is given by [7]

$$K = D_S \gamma \nu / n^2 k_B T, \quad D_S = \overline{D_{S_0}} e^{-Q_a / k_B T} \quad (7)$$

where  $D_S$  [15] is the surface self-diffusivity,  $Q_a$  is the activation energy,  $\gamma$  is the surface free energy per unit area and  $\nu$  is the areal density of diffusing atoms.

In the linear regime, periodical stripes with

$$|\vec{k}| = \sqrt{-\nu/2K}, \quad \nu = \min(\nu_x, \nu_y) \quad (8)$$

have the highest growth rate. Consequently, for  $\nu = \nu_x < 0$  the surface will be dominated by ripples along the  $\hat{y}$ -axis ( $\vec{k} \parallel \hat{x}$ ) and for  $\nu = \nu_y < 0$  by ripples parallel to the  $x$ -axis ( $\vec{k} \parallel \hat{y}$ ).

In the case of the laser material interaction, we assume that the photons loose their energy in a similar stochastic process. The widths  $\alpha$  and  $\beta$  of the Gauss distribution (2) are equal because the target is isotropic. The incident energy flux  $\epsilon \Psi(\vec{r})$  is now given by  $a\gamma |\vec{S}_2 \vec{n}|$ , where

$a$  has the meaning of an average penetration depth,  $\gamma$  is the absorption coefficient of the material and  $\vec{S}_2$  is the Poynting vector of the refracted beam. The product  $a\gamma$  represents the fraction of the transmitted energy that will be absorbed, that is, in an ionic picture, *scattered* by the material. Using the Fresnel equations, the incident flux can be written in terms of the laser intensity  $I_0 = |\vec{S}_1|$  and of the transmission coefficient  $T$

$$\epsilon\Psi(\vec{r}) \rightarrow a\gamma \frac{|\vec{S}_2\vec{n}|}{|\vec{S}_1\vec{n}|} \frac{|\vec{S}_1\vec{n}|}{|\vec{S}_1|} |\vec{S}_1| = a\gamma I_0 T(\vec{r}, \phi) \cos \phi. \quad (9)$$

In the next step we insert the energy flux (9) and the Gaussian distribution (2) into Eq. (3) to compute the local erosion rate. To evaluate the integral (3), we extend the Taylor expansion (4) to its complete form

$$h \cong -\frac{1}{2} \left( \frac{x^2}{R_X} + \frac{y^2}{R_Y} \right) - \frac{xy}{R_{XY}}, \quad (10)$$

where  $1/R_{XY} = -\partial^2 h / \partial x \partial y$ .

We call the last term in Eq. (10) a “rotational” correction. In their original model, Bradley and Harper have neglected it and could therefore only describe patterns growing along the  $x$ - or the  $y$ -axis. With this term the stability analysis can still be reduced to the case of Bradley and Harper, but in a reference frame rotated by an angle  $\Theta$  to the original one. Following the notation style of Eq. (6) and denoting by  $\nu_{xy}$  the coefficient of  $h_{xy}$ , the angle  $\Theta$  is determined by

$$\nu_{xy} \cos 2\Theta = (\nu_x - \nu_y) \sin 2\Theta. \quad (11)$$

We perform the transition (5) to the coordinate frame of the laboratory and scale the time and the space according to

$$x = ax', \quad y = ay', \quad t = \frac{\sqrt{2\pi}a}{\Lambda\gamma I_0}. \quad (12)$$

to obtain

$$\begin{aligned} \dot{h} = & -v_0 + \mu h_x + \nu_x h_{xx} + \nu_y h_{yy} + \nu_{xy} h_{xy} + \frac{1}{2} \lambda_x h_x^2 \\ & + \frac{1}{2} \lambda_y h_y^2 + \nu_{10100} h_x h_{xx} + \nu_{10010} h_x h_{yy} + \\ & \nu_{10001} h_x h_{xy} + \nu_{00200} h_{xx}^2 + \nu_{00020} h_{yy}^2 + \nu_{00002} h_{xy}^2 \\ & + \nu_{00110} h_{xx} h_{yy} + \nu_{00101} h_{xx} h_{xy} + \nu_{00011} h_{yy} h_{xy} \\ & - B\Delta^2 h. \end{aligned} \quad (13)$$

The tuples  $ijklm$  in  $\nu_{ijklm}$  describe the product  $h_x^i h_y^j h_{xx}^k h_{yy}^l h_{xy}^m$  these coefficients belong to. Except for  $B$ , all the coefficients in Eq. (13) have the form  $\{, \} = \sigma \exp[-\frac{\sigma^2}{2} \cos^2 \theta] f_{\{, \}}(n, \theta, \varphi)$ , with  $\sigma = a/\alpha$ .

Fig. 2 shows a 3D plot of  $-\nu_x$ ,  $-\nu_y$  and  $-\nu_{xy}$  against the angle of incidence  $\theta$  and the polarization  $\varphi$ . We chose

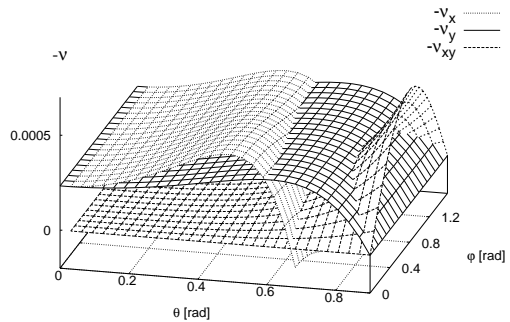


FIG. 2: Plot of  $\nu_x$ ,  $\nu_y$  and  $\nu_{xy}$  against the angle of incidence  $\theta$  and the polarization  $\varphi$ .  $\sigma = 4$ ,  $n = 1.47$

$\sigma=4$ ,  $B = 1.2 \cdot 10^{-4}$  and  $n=1.47$ , the refraction index of BaF<sub>2</sub> at  $\lambda \sim 750$  nm. As shown in the previous section, the larger of  $-\nu_x > 0$  and  $-\nu_y > 0$  determines the prevailing pattern and  $\nu_{xy}$  will rotate this pattern by an angle  $\Theta$  (Eq. (11)).

We see that there is actually only a small region between  $\theta_{\min}$  and  $\theta_{\max}$ , where the ripple orientation changes with the light polarization. In our case  $\theta_{\min}$  was  $29.64^\circ$  and  $\theta_{\max} = 34.04^\circ$ . For angles smaller than  $\theta_{\min}$  the ripples should always be perpendicular to the surface component of the laser beam, where as for angles larger than  $\theta_{\max}$  they should be parallel. The width of this region is usually between 1 and 5 degrees, increasing with increasing  $n$ . Its position varies slightly with  $\sigma$ , but strongly with  $n$ . Smaller  $n$ 's and larger  $\sigma$ 's will move it towards angles of up to  $50 - 60^\circ$ .

The present work is an attempt to investigate the occurrence of newly discovered laser induced periodic surface structures [6] by means of the Bradley et al. [7] and Cuerno et al. [8] model. Based on Sigmund's stochastic theory of sputtering [12], this model has managed to explain in a unified framework most of the dynamic and scaling behaviors observed experimentally at ion bombardment of surfaces. It eventually traces the origin of ripple formation down to the instability caused by the competition between surface roughening (so called negative surface tension) and surface diffusion (the positive surface tension).

The use of the Fresnel equations and the inclusion of the  $\nu_{xy}(\partial^2 h / \partial x \partial y)$  term to the Kuramoto-Sivashinsky equation, have allowed us to confirm the experimentally observed continuous change of the ripple orientation with the laser polarization. However, our model predicts that this should only happen for angles of incidence confined in a small range between  $\theta_{\min}$  and  $\theta_{\max}$ . In our simulations this range corresponded to  $29 - 34^\circ$ , but could move up to  $53 - 55^\circ$ .

The role of the local laser intensity can also be explained. According to Eq. (7), for local temperatures

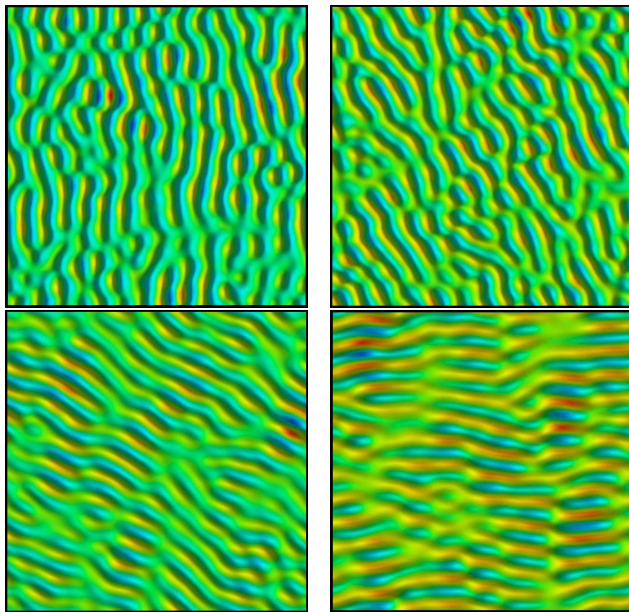


FIG. 3: Surface topography for  $\theta=31.8^\circ$  and  $\varphi=0^\circ, 30^\circ, 60^\circ$  and  $90^\circ$  respectively (upper-left to lower-right).

$T_{\text{local}}$  below  $Q_a$ ,  $K$  is a monotonically increasing function of  $T_{\text{local}}$  and thus of the laser intensity  $I_{\text{local}}$ . A first estimation yields  $Q_a > 0.53$  eV [22], much larger than the melting point of  $\text{BaF}_2$  ( $1280^\circ\text{C} \approx 0.13$  eV). The periodicity  $2\pi/|\vec{k}|$  of the ripples (Eq. (8)) is thus an increasing function of  $I_{\text{local}}$ , just like in Fig. 1(a).

At normal incidence, all patterns with the wave vector satisfying  $|\vec{k}| = \sqrt{-\nu/2B}$  can occur with equal probability. The symmetry break has therefore been looked for and traces of it have been found in the 3<sup>rd</sup> order terms. However, further investigation is needed, as we have not been able to simulate any ripples yet.

It is well known that the spacing of the structures described by the KS equation increases with time according to  $\lambda \sim t^\gamma$ . The value of  $\gamma$  varies with different experimental conditions [16, 17, 18] and different numerical simulations [13, 14, 19]. Considering that the exposure times varied across the experiments, an unknown value of  $\gamma$  makes the direct quantitative comparison of the numerical simulations with the experiment impossible. A comprehensive study of the time behavior of the structures is therefore a further requirement for their understanding.

Frost et al. have recently shown that the compound nature of a material can considerably influence the scaling behavior of the surface structures in the early stages of ion sputtering [16]. Considering the extreme conditions of the laser ablation, the loss of atoms is with high probability different for Ba and F, so that a spatially varying concentration of adatoms on the surface would arise. Mayr et al. have shown that surface diffusion driven by a concentration gradient of the adatoms is

able to generate structure coarsening [20]. According to Frost et al., this type of coarsening would be one of the causes for the deviation from the KS predicted scaling behavior they have observed in the early stages of  $\text{Ar}^+$  sputtering of InP surfaces.

Further experiments with rotating targets or circular polarized light could also confirm the common nature of this new type of LIPSS and of the ion sputtering processes. Studying the topography of simultaneously rotated and  $\text{Ar}^+$  ion sputtered InP surfaces, Frost et al. have been able to find structures of highly hexagonal symmetry [16].

I. Georgescu would like to thank Mario de Menech for helpful discussions.

---

\* Current address Max-Planck-Institut für Physik komplexer Systeme, Nöthnitzer Str. 38, 01187 Dresden, Germany.; Electronic address: george@pks.mpg.de

- [1] H. M. van Driel, J. E. Sipe, and J. F. Young, Phys. Rev. Lett. **49**, 1955 (1982).
- [2] J. E. Sipe, J. F. Young, J. S. Preston, and H. M. van Driel, Phys. Rev. B **27**, 1141 (1983).
- [3] J. F. Young, J. S. Preston, H. M. van Driel, and J. E. Sipe, Phys. Rev. B **27**, 1155 (1983).
- [4] J. F. Young, J. E. Sipe, and H. M. van Driel, Phys. Rev. B **30**, 2001 (1984).
- [5] S. E. Clark and D. C. Emmony, Phys. Rev. B **40**, 2031 (1989).
- [6] F. Costache, M. Henyk, and J. Reif, Appl. Surf. Sci. **186**, 352 (2002).
- [7] R. M. Bradley and J. M. E. Harper, J. Vac. Sci. Technol. A **6**, 2390 (1988).
- [8] R. Cuerno and A.-L. Barabási, Phys. Rev. Lett. **74**, 4746 (1995).
- [9] F. Costache, M. Henyk, and J. Reif, Appl. Surf. Sci. **203**, 486 (2003).
- [10] J. Reif, F. Costache, M. Henyk, and S. V. Pandelov, Appl. Surf. Sci. **197-198**, 891 (2002).
- [11] M. Henyk, N. Vogel, D. Wolframm, A. Tempel, and J. Reif, Appl. Phys. A **69**, 355 (1999).
- [12] P. Sigmund, Physical Review **194**, 383 (1969).
- [13] M. Kardar, G. Parisi, and Y.-C. Zhang, Phys. Rev. Lett. **56**, 889 (1986).
- [14] K. B. Lauritsen, R. Cuerno, and H. A. Makse, Phys. Rev. E **54**, 3577 (1996).
- [15] G. Neumann and W. Hirschwald, Zeitschrift für Physikalische Chemie Neue Folge **81**, 163 (1972).
- [16] F. Frost, A. Schindler, and F. Bigl, Phys. Rev. Lett. **85**, 4116 (2000).
- [17] S. Habenicht and K. P. Lieb, Phys. Rev. B **65**, 115327 (2002).
- [18] S. Habenicht, W. Bolse, and K. P. Lieb, Phys. Rev. B **60**, R2200 (1999).
- [19] J. T. Drotar, Y.-P. Zhao, T.-M. Lu, and G.-C. Wang, Phys. Rev. E **59**, 177 (1999).
- [20] S. G. Mayr, M. Moske, and K. Samwer, Phys. Rev. B **60**, 16950 (1999).
- [21] R. Feynman, R. B. Leighton, and M. L. Sands, *The Feyn-*

*man lectures on physics*, vol. II (Addison-Wesley, 1964),  
8-3 The electrostatic energy of an ionic crystal.

[22]  $Q_a$  is additively composed of  $H_{Fa}$  and  $H_{Ma}$ , the formation and migration energy of an adatom [15]. We have

numerically evaluated  $H_{Ma}$  for the (110) surface of BaF<sub>2</sub> and obtained 0.53 eV [21].